CALIBRATION OF PIEZO-IMPEDANCE TRANSDUCERS FOR STRENGTH PREDICTION AND DAMAGE ASSESSMENT OF CONCRETE

Chee Kiong SOH [1] and Suresh BHALLA [2]

Division of Structures and Mechanics

School of Civil and Environmental Engineering

Nanyang Technological University

50 Nanyang Avenue

Singapore 639798

Short Title : Calibration of Piezo-Transducers

Classification No. : 81.70.Yp

(Based on Physics and Astronomy Classification Scheme)

[1] Professor (**E-mail**: csohck@ntu.edu.sg, **Phone:** (65) 6 790-5306, **Fax:** (65) 6 791-5093

[2] Project Officer (E-mail: sbhalla@.ntu.edu.sg)

ABSTRACT

This paper presents a new approach for non-destructive evaluation (NDE) of concrete, covering both strength prediction and damage assessment, using the electro-mechanical impedance (EMI) technique. A new empirical method is proposed to determine *in situ* concrete strength non-destructively using admittance signatures of surface bonded piezo-impedance transducers. This is followed by 'identification' of appropriate impedance parameters for concrete. The identified parameters are found to be sensitive to structural damages as well as to concrete strength gain during curing. Comprehensive tests were conducted on concrete specimens up to failure to empirically calibrate the 'identified' system parameters with damage severity. An empirical fuzzy probabilistic damage model is proposed to quantitatively predict damage severity in concrete based on variation in the identified equivalent stiffness.

KEY WORDS: Electro-mechanical impedance (EMI) technique; non-destructive evaluation (NDE); structural health monitoring (SHM); strength; damage; admittance.

1. CONVENTIONAL NDE METHODS FOR CONCRETE

In general, from the point of view of non-destructive evaluation (NDE), concrete technologists are interested in: (a) concrete strength determination, and (b) concrete damage detection. Special importance is attached to strength determination of concrete because its elastic behaviour and to some extent service behaviour can be predicted from its strength characteristics. Commonly used non-destructive strength estimation methods are the surface hardness method, the penetration technique, the pullout test, the rebound hammer method, the resonant frequency method and the ultrasonic pulse velocity test (Malhotra 1976; Bungey 1982). These methods typically measure certain properties of concrete from which an estimate of its strength, durability and elastic parameters can be derived. Hence, they cannot be expected to yield absolute values of strength. The surface hardness method, for example, is based on the principle that the strength of concrete is proportional to its surface hardness. However, these strength prediction methods share many limitations. For example, the calibration charts of the surface hardness method, the rebound method and the penetration technique are valid for the particular type of the cement and aggregates used and the age and moisture content of the specimen. In addition, the results are not very reproducible. The penetration and the pull-out techniques cause a small amount of damage to the concrete surface, which must be repaired. The resonant frequency method and the ultrasonic pulse velocity technique demand that the transducers must be placed on the opposite faces of the component for accurate results. Very often, this is not possible and thus limits the application of the two techniques.

The other aspect of NDE, namely damage detection, is conventionally carried out by *global* and *local* techniques. The global techniques rely on global structural response for damage identification. For example, in global dynamic techniques (Pandey and Biswas 1991,

1994; Zimmerman and Kaouck 1994; Farrar and Jauregui 1998; Aktan *et al.* 2000), the structure is subjected to low frequency excitations and from the resulting structural response, the first few mode shapes and their corresponding natural frequencies are extracted to deduce the location and the severity of structural damage. The main drawback of these techniques is that they rely on relatively small number of the first few modes, which, being global in nature, are not very sensitive to localized incipient damage. It could be possible that a damage large enough to be detected by these techniques may already exist critically in many parts of the structure.

The *local* damage detection techniques, such as ultrasonic wave propagation, impact echo and acoustic emission techniques, on the other hand, employ localized structural interrogation for damage detection. In *ultrasonic* techniques, typically, high frequency elastic waves are propagated into the monitored structural component. The waves reflect back when encountering any crack. The crack location is estimated from the time difference between the applied and the reflected waves. The ultrasonic techniques exhibit much higher damage sensitivity than the global techniques. However, they typically employ large and expensive transducers and render the structure unavailable for service throughout the duration of the test. The measurement data is collected in time domain and requires complex processing. Since ultrasonic waves cannot be induced at right angles to the surface, they cannot detect transverse surface cracks (Giurgiutiu and Rogers 1997). In addition, they do not lend themselves to automated use since experienced technicians are required to interpret the data.

In the *acoustic emission* technique, elastic waves generated by plastic deformations (such as at the tip of a newly developed crack), moving dislocations and disbonds are utilized for analysis and detection of structural defects. This technique requires stress or chemical activity to generate elastic waves. However, the main problem for damage identification is the

existence of multiple travel paths from the source to the sensors. Also, contamination by electrical interference and ambient mechanical noise degrades the quality of the emission signals (Park *et al.* 2000; Kawiecki 2001).

In *impact echo* testing, a stress pulse is introduced into the interrogated structural component using an impact source. As the pulse propagates through the component, it is reflected by cracks and disbonds. The reflected waves are measured and analyzed to deduce the location of the cracks or disbonds. Though the technique is very good for detecting large-size voids and delaminations, it is insensitive to small sized cracks (Park *et al.* 2000).

A common drawback of the *local* techniques is that probes, fixtures and other accessories are required to be physically carried around the test-structure for recording the data. Often, this not only prevents autonomous application of the techniques, but may also demand the removal of existing finishes or covers such as false ceilings. As it is impractical to freely move the probe everywhere, these techniques are often applied at few selected probable damage locations (often based on preliminary visual inspection or past experience), which is almost tantamount to knowing the damage location *a priori*.

The electro-mechanical impedance (EMI) technique, on the other hand, offers to interface between the *global* and the *local* techniques, thereby enabling a more cost-effective and hassle free alternative for both strength estimation and damage detection of concrete structures.

2. ELECTRO-MECHANICAL IMPEDANCE (EMI) TECHNIQUE

During the last few years, the EMI technique has demonstrated its potential for cost-effective structural health monitoring (SHM) for a wide variety of engineering structures (Sun *et al.* 1995; Ayres *et al.* 1998; Soh *et al.* 2000; Park *et al.* 2000, 2001; Giurgiutiu and Zagrai,

2000, 2002; Bhalla and Soh, 2003, 2004a). In principle, this technique is similar to the conventional global vibration techniques. The major difference, however, is only with respect to the frequency range employed, which is typically 30-400 kHz in the EMI technique, against less than 100 Hz in the global vibration techniques. High vibration frequency is achieved by electrically exciting a piezoelectric-ceramic (PZT) patch, surface bonded to the monitored structure, by means of an impedance analyzer. The PZT patches are made up of 'piezoelectric' materials, which generate surface charges in response to applied mechanical stresses and conversely undergo mechanical deformations in response to applied electric fields. Hence, when the bonded PZT patch is electrically excited, it produces deformations in the surrounding local area of the host structure. The response of this area is transferred back to the PZT wafer in the form of admittance function, comprising of the conductance (the real part) and the susceptance (the imaginary part). These electrical 'signatures' of the structure (in frequency domain), contain vital information concerning the phenomenological nature of the structure. Hence, the same PZT patch acts as an actuator as well as a sensor concurrently.

Liang *et al.* (1994) first proposed the impedance approach to model PZT-structure electromechanical interaction in 1D structures. Bhalla and Soh (2004b) extended the 1D impedance formulations to 2D structures by introducing the concept of 'effective impedance'. The related physical model is shown in Fig. 1 for a square PZT patch of length '2l' and thickness 'h'. In this approach, the PZT-structure interaction is represented in the form of distributed boundary force 'f' per unit length (rather than end point forces as in previous approaches), varying harmonically with time. This harmonic force causes harmonic planar deformations in the PZT patch, leading to variations in its overall area. The 'effecive mechanical impedance' of the patch can be defined as

$$Z_{a,eff} = \frac{\oint_S \vec{f}.\hat{n}\,ds}{\dot{u}_{eff}} = \frac{F}{\dot{u}_{eff}} \tag{1}$$

where $\hat{n}$ is the unit vector normal to the boundary and '*F*' represents the overall planar force (or effective force) causing area deformation of the PZT patch. $u_{eff} = \delta A/p_o$ is the 'effective displacement' of the PZT patch, where δA denotes the change in surface area of the patch and p_o its perimeter in the undeformed condition. Differentiation of the effective displacement with respect to time yields the effective velocity, $\dot{u}_{eff}$. The effective drive point (EDP) impedance of the host structure can also be defined on similar lines, by applying force on the surface of the host structure, along the boundary of the proposed location of the PZT patch (however ignoring the patch). The overall planar force F is related to the EDP impedance of the structure by

$$F = \oint_S \vec{f}.\hat{n}ds = -Z_{s,eff}\dot{u}_{eff} \tag{2}$$

Solving the governing 2D wave equation and introducing new correction factors, Bhalla and Soh (2004b, 2004c) derived the following expression for the complex electro-mechanical admittance $\overline{Y}$

$$\overline{Y} = G + Bj = 4\omega j \frac{l^2}{h}\left[\overline{\varepsilon_{33}^T} - \frac{2d_{31}^2\overline{Y^E}}{(1-\nu)} + \frac{2d_{31}^2\overline{Y^E}}{(1-\nu)}\left(\frac{Z_{a,eff}}{Z_{s,eff}+Z_{a,eff}}\right)\overline{T}\right] \tag{3}$$

where ω is the angular frequency, d_{31} the piezoelectric strain coefficient, $\overline{Y^E} = Y^E(1+\eta j)$ the complex Young's modulus of elasticity of the PZT patch (at constant electric field), $\overline{\varepsilon_{33}^T} = \varepsilon_{33}^T(1-\delta j)$ the complex electric permittivity of the PZT material (at constant stress) and ν the Poisson's ratio. η and δ denote respectively the mechanical loss factor and the dielectric loss factor of the PZT patch. The term $\overline{T}$ is the complex tangent ratio, ideally equal to

$\{\tan(\kappa l)/\kappa l\}$, where $\kappa = \omega\sqrt{\rho(1-\nu^2)/\overline{Y^E}}$ is the wave number. However, in actual practice, it requires correction to accommodate deviation of the PZT patch from the ideal behavior and can be expressed as

$$\overline{T} = \begin{cases} \dfrac{\tan(C\kappa l)}{C\kappa l} & \text{for single-peak behaviour.} \\ \dfrac{1}{2}\left(\dfrac{\tan(C_1\kappa l)}{C_1\kappa l} + \dfrac{\tan(C_2\kappa l)}{C_2\kappa l} \right) & \text{for twin-peak behaviour.} \end{cases} \tag{4}$$

The constants C_1 and C_2, (or C) and whether the patch conforms to 'single-peak' or 'twin-peak' behavior, can be determined from the signatures of the PZT patches in 'free-free' condition prior to their bonding on the host structure (Bhalla and Soh 2004b). Further, Z_a which represents the mechanical impedance of the PZT patch (in short-circuited condition), is mathematically given by

$$Z_{a,eff} = \frac{2h\overline{Y^E}}{j\omega(1-\nu)\overline{T}} \tag{5}$$

As seen from Eq. (3), any damage to the structure (i.e. any change in mechanical impedance '$Z_{s,eff}$') manifests itself as a deviation in the admittance signature, thereby providing an indication of the damage. The EMI technique has far greater sensitivity to structural damages than the conventional global vibration techniques. It is typically of the order of the 'local' ultrasonic techniques. However, unlike the local techniques, the EMI technique does not warrant expensive transducers and hardware, and also does not necessitate any probe to be physically moved or the structure to be placed out of service. The data acquisition is much more simplified than the traditional accelerometer-shaker combination employed in the global vibration techniques. Hence, the EMI technique bridges the gap between the global and the local techniques (Park et al 2003).

However, in-spite of key advantages, no ready calibration is currently available so as to realistically predict damage level from the measured signatures. Till date, all the damage quantification techniques are non-parametric and statistical in nature, and utilize the real component of the signature alone. The following sections of this paper highlight a new application of the EMI technique and the associated impedance modelling for predicting concrete strength, monitoring concrete curing and quantitative damage prediction.

3. CONCRETE STRENGTH EVALUATON USING EMI TECHNIQUE

Eq. (3) predicts the electrical admittance across the terminals of a square PZT patch surface bonded to any structure. From this relationship, admittance spectra can be derived for a 'free' and a 'perfectly clamped' PZT patch, by substituting $Z_{s,eff}$ equal to 0 and ∞ respectively. Fig. 2 displays the admittance spectra (0-1000 kHz), corresponding to these boundary conditions, for a PZT patch 10x10x0.3mm in size, conforming to grade PIC 151 (PI Ceramic 2004). It is observed from this figure that the three resonance peaks corresponding to planar PZT vibrations vanish upon clamping the patch. The act of bonding a PZT patch on the surface of any structure tends to similarly restrain the PZT patch. However, the level of clamping is intermediate of these two extreme conditions and therefore, the admittance curves are likely to lie in between the two extreme curves, depending on the stiffness (or strength) of the component and the bonding layer.

In order to test the feasibility of predicting concrete strength using this principle, identical PZT patches (measuring 10x10x0.3mm, grade PIC 151: PI Ceramic 2004), were bonded on the surface of concrete cubes, 150x150x150mm in size. At the time of casting, the proportions of the various constituents were adjusted so that different characteristic strengths would be achieved. After casting, a minimum curing period of 28 days was observed for all

the specimens except two, for which it was kept one week only so as to achieve relatively low strength. In order to achieve identical bonding conditions, two optical fiber pieces, 0.125mm in diameter, were first laid down parallel to each other on the concrete surface, as shown in Fig. 3 (a). A layer of epoxy adhesive (RS 850-940, RS Components 2004) was then applied on the concrete surface and the PZT patch was placed on it. Light pressure was maintained over the assembly using a small weight and the setup was left undisturbed in this condition at room temperature for 24 hours to facilitate complete curing of the adhesive. This procedure ensured a uniform thickness of 0.125mm of the bonding layer in all the specimens tested. Fig. 4 shows the conductance and susceptance plots obtained from the PZT patches bonded to concrete cubes of five different strengths. The strengths indicated on the figure were determined experimentally by subjecting the cubes to cyclic loading on a universal testing machine (UTM). The test procedure will be covered in the next section. The figure also shows the analytical curves for PZT patch in free as well as perfectly clamped conditions.

It is apparent from the figures that the first peak frequency (see Fig. 2a) gradually shifts to the right as the strength of concrete increases. This shifting is on account of the additional stiffening action due to bonding with concrete, the level of stiffening being directly related to the concrete strength. Fig. 5 shows a plot between the observed first resonant frequency and measured concrete strength for data pertaining to a total of 17 PZT patches, bonded to a total of 11 concrete cubes. At least two cubes were tested corresponding to each strength and averaged values of the observed frequency were used to obtain the plot. Free PZT curve was used to obtain the data point corresponding to zero strength. From regression analysis, following empirical relationship was derived between concrete strength (S) and the observed first resonant frequency

$$S(MPa) = 0.0089 f^2 - 2.6657 f + 196.94 \qquad (6)$$

where the resonant frequency, f, is measured in kHz. This empirical relationship can be used to evaluate concrete strength non-destructively for low to high strength concrete (10MPa < S < 100MPa). It should be mentioned that good correlation was not found between concrete strength and the second and the third peaks (see Fig. 2). This is because at frequencies higher than 500 kHz, the PZT patches become sensitive to their own conditions rather than the conditions of the structure they are bonded to (Park et al 2003).

It should be noted that the strength considered in our study is obtained by cyclic compression tests, which is expected to be lower than that obtained by the standard testing procedure. Also, the empirical relationship (Eq. 6) will depend on the type and size of the PZT patches and the type and thickness of the bonding layer. It may also depend on the type of aggregates and the type of cement used. Thus, Eq. (6) should not be considered as a universal relationship. It is therefore recommended that similar calibration should be first established in the laboratory for the particular concrete to be investigated before using the proposed method in the field.

Although the tests reported in this study were carried out on 150mm cubes, the empirical relationship represented by Eq. (6) can also be conveniently used for life-sized structures since the zone of influence of the PZT patches is usually very small in concrete. The main advantage in the proposed technique is that there is no requirement for the availability of two opposite surfaces as in the case of the resonant frequency method and the ultrasonic pulse velocity method. Besides, no expensive transducers or hardware are warranted.

4. EXTRACTION OF DAMAGE SENSITIVE CONCRETE PARAMETERS FROM ADMITTANCE SIGNATURES

4.1 Decomposition of Coupled Electro-Mechanical Admittance

The electro-mechanical admittance (given by Eq. 3) can be decomposed into two components as

$$\bar{Y} = \underbrace{4\omega j \frac{l^2}{h}\left[\overline{\varepsilon_{33}^T} - \frac{2d_{31}^2 \overline{Y^E}}{(1-\nu)}\right]}_{\textbf{Part I}} + \underbrace{\frac{8\omega d_{31}^2 \overline{Y^E} l^2}{h(1-\nu)}\left(\frac{Z_{a,eff}}{Z_{s,eff}+Z_{a,eff}}\right)\overline{T}\, j}_{\textbf{Part II}} \tag{7}$$

It can be observed that the first part solely depends upon the parameters of the PZT patch and is independent of the host structure. The structural parameters make their presence felt in part II only, in the form of the EDP structural impedance, $Z_{s,eff}$. Therefore, Eq. (7) can be written as

$$\bar{Y} = \overline{Y_P} + \overline{Y_A} \tag{8}$$

where $\overline{Y_A}$ is the 'active' component and $\overline{Y_P}$ represents the 'passive' component. $\overline{Y_P}$ can be further broken down into real and imaginary parts by expanding $\overline{\varepsilon_{33}^T} = \varepsilon_{33}^T(1-\delta j)$ and $\overline{Y^E} = Y^E(1+\eta j)$, and hence can be expressed as

$$\overline{Y_P} = G_P + B_P j \tag{9}$$

where $G_P = \frac{4\omega l^2}{h}\left\{\delta\varepsilon_{33}^T + K\eta\right\}$ and $B_P = \frac{4\omega l^2}{h}\left\{\varepsilon_{33}^T - K\right\}$ (10)

and $$K = \frac{2d_{31}^2 Y^E}{(1-\nu)} \tag{11}$$

G_P and B_P can be predicted with reasonable accuracy by recording the conductance and the susceptance signatures of the PZT patch in 'free-free' condition, prior to its bonding to the

host structure (Bhalla and Soh 2004b). Hence, the PZT contribution can be filtered off from the raw signatures and the active component deduced as

$$\overline{Y_A} = \overline{Y} - \overline{Y_P} \tag{12}$$

In the complex form, the active component can be expressed as

$$\overline{Y_A} = G_A + B_A j = \frac{8\omega d_{31}^2 \overline{Y^E} l^2}{h(1-\nu)} \left(\frac{Z_{a,eff}}{Z_{s,eff} + Z_{a,eff}} \right) \overline{T} j \tag{13}$$

It has been demonstrated by Bhalla and Soh (2003), using 1D interaction model, that the elimination of the passive component renders the admittance signatures more sensitive to structural damages.

4.2 Extraction of Structural Mechanical Impedance

Substituting $\overline{Y^E} = Y^E(1+\eta j)$ and $\overline{T} = r + tj$ into Eq. (13), and rearranging the various terms, we obtain

$$M + Nj = \left(\frac{Z_{a,eff}}{Z_{S,eff} + Z_{a,eff}} \right) (R + Sj) \tag{14}$$

where

$$M = \frac{B_A h}{4\omega K l^2} \quad \text{and} \quad N = -\frac{G_A h}{4\omega K l^2} \tag{15}$$

$$R = r - \eta t \quad \text{and} \quad S = t + \eta r \tag{16}$$

Further, expanding $Z_{S,eff} = x + yj$ and $Z_{a,eff} = x_a + y_a j$, and upon solving, the real and imaginary components of the EDP structural impedance can be obtained as

$$x = \frac{M(x_a R - y_a S) + N(x_a S + y_a R)}{M^2 + N^2} - x_a \tag{17}$$

$$y = \frac{M(x_a S + y_a R) - N(x_a R - y_a S)}{M^2 + N^2} - y_a \tag{18}$$

The simple computational procedure outlined above enables the determination, from the measured data, of the drive point mechanical impedance of the structure, $Z_{s,eff} = x + yj$, at a particular angular frequency ω, without demanding any a-priori information governing the phenomenological nature of the structure. The only requirement is an 'updated' model of the PZT patch, which can be derived from preliminary specifications of the PZT patch and by recording its admittance signatures in the 'free-free' condition, prior to bonding to the host structure. The next section will present a simple procedure to derive system parameters from the structural EDP impedance. In all these computations, the term $\overline{T}$ (which plays a significant role), depends upon $\tan(\kappa l)/\kappa l$ (see Eq. 4), where κl is a complex number. It is essential to determine this quantity precisely, by the theory of complex algebra (Kreyszig 1996). Further, it should be noted that $|x| > |x_a|$ and $|y| > |y_a|$ in order to ensure smooth computations; else, the extracted impedance spectra might exhibit false peaks.

4.3 Structural Identification in Concrete

Consider again the concrete cubes, 150x150x150mm in size, instrumented with square PZT patches, 10x10x0.3mm in size, conforming to grade PIC 151 (PI Ceramic 2004). Using the procedure outlined by Bhalla and Soh (2004b), updated 'models' were obtained for five representative PZT patches of the set by recording their signatures in 'free-free' condition. Table 1 lists the key averaged PZT parameters for the batch. For the other less important parameters, the values supplied by the manufacturer were used. Using the computational procedure outlined earlier, the impedance parameters of the concrete cubes (x and y) were extracted from the admittance signatures of the bonded PZT patches in the frequency range 60-100 kHz. The real and imaginary components of the extracted mechanical impedance were found to exhibit a response similar to that of a parallel spring damper

combination as shown in Fig. 6. For concrete cube with a strength of 43 MPa (designated as C43), the system parameters were identified to be $k = 5.269 \times 10^7$ N/m and c = 12.64 Ns/m.. Fig. 7 shows a comparison between the experimental impedance spectra and that corresponding to the parallel spring damper combination with $k = 5.269 \times 10^7$ N/m and c = 12.64 Ns/m . A good agreement can be observed between the two. The experimental values of "x", which seem to have a small slope (Fig. 7a), can be assumed constant for the small frequency range considered. Similar trends were observed for other concrete cubes also.

The concrete cubes were subjected to cyclic loading in an experimental set-up shown in Fig. 8. The PZT patches instrumented on the cube were wired to an impedance analyzer, which was controlled using the personal computer labelled as PC1 in the figure. The strain gauge was wired to a strain recording data logger, which was in-turn hooked to another personal computer marked as PC2, which also controlled the operation of the UTM. Any given test cube was first loaded in compression at a rate of 330 kN/min until the first predetermined load. It was then unloaded and the conductance and susceptance signatures were acquired. In the next cycle, the cube was loaded to the next higher level of load and the signatures were again acquired after unloading. This loading, unloading and signature acquisition process was repeated until failure. Thus, damage was induced in a cyclic fashion. Fig. 9 shows the conductance signature obtained from the PZT patch bonded to cube C43 (Strength = 43MPa) at various load ratios (i.e. applied load divided by failure load) during the test. Deviation in the conductance signature implied the occurrence of damage in the specimen. Similar changes were observed for other test specimens as well. Typical load histories from four cubes designated as C17 (Strength = 17MPa), C43 (Strength = 43MPa), C54 (Strength = 54MPa) and C86 (Strength = 86MPa), are shown in Fig. 10. From this figure, it is observed that the secant modulus progressively diminishes with the number of

load cycles. At the same time, the extracted equivalent spring stiffness, calculated from the recorded admittance signatures, was found to diminish proportionally. Fig. 11 shows the plots of the loss of secant stiffness against the loss of equivalent spring stiffness for the four cubes C17, C43, C52 and C86. A good correlation can be observed between the loss of secant modulus and the loss of equivalent stiffness as identified by the piezo-impedance transducers. From these results, it is evident that equivalent spring stiffness can be regarded as a damage sensitive parameter and can be utilized to quantitatively predict the extent of damage in concrete. It should be noted that the equivalent spring stiffness is obtained solely from the signatures of the piezo-impedance transducers. No information about concrete specimen is warranted *a priori.*

It should also be mentioned that the extracted equivalent damping was found to increase with damage. This was expected, since damping is known to increase with the development of cracks in concrete. Fig. 12 shows the plot of increase in equivalent damping with damage progression for cube C43. Also shown is the loss in equivalent stiffness with load ratio. However, in most other cubes, no consistent pattern was found with respect to damping. Only a phenomenal increase near failure was observed. For this reason, the equivalent stiffness was selected as the damage indicative parameter due to its progressive decrement with damage progression in all the cubes tested. Development of an empirical damage model based on the equivalent spring stiffness is covered in the latter part of this paper.

5. MONITORING OF CONCRETE CURING USING EXTRACTED EQUIVALENT STIFFNESS

In order to evaluate the feasibility of the ‘identified’ equivalent spring stiffness in monitoring concrete curing, a PZT patch, 10x10x0.3mm in size (grade PIC 151, PI Ceramic

2004) was instrumented on a concrete cube, measuring 150x150x150mm in size. Again, a bond layer thickness of 0.125mm was achieved with the aid of optical fibre pieces. The instrumentation was done three days after casting the cube. The PZT patch was periodically interrogated for the acquisition of electrical admittance signatures and this was continued for a period of one year.

Figs. 13 and 14 respectively show the short term and the long term effects of ageing on the conductance signatures of the PZT patch in the frequency range 100-150 kHz. It is observed that, with ageing, the peak shift rightwards and at the same time getting sharper. This trend is exactly opposite to the trend usually observed during compression tests, where the peaks shift towards the left. The shifting of the resonance peak towards the right in the present case indicates that the stiffness (and hence the strength) increases with time. The phenomenon of peak getting sharper with time suggests that the material damping is reducing (concrete was initially 'soft'). It is a well known fact that major damping in concrete occurs in the matrix, some in the interfacial boundaries and a small fraction in the aggregates. Moisture in the matrix is the major contributor to damping (Malhotra 1976). Hence, with curing, as moisture content drops, the damping in concrete tends to fall down.

It should be noted that the particular peak in this figure is the resonance peak of the structure. It should not be confused with the resonance peak of the PZT patch, such as that shown in Fig. 2. As concrete strength increases, the resonance peak of the PZT patch subsides due to the predominance of structural interaction. The structural resonance peak (Figs. 13 and 14), on the other hand, tends to get sharper. In other words, increasing structural stiffness tends to 'dampen' PZT resonance and 'sharpen' the host structure's resonance peak.

In order to quantitatively describe the phenomenon, the equivalent spring stiffness of the cube identified by the PZT patch was worked out in the frequency range 60-100 kHz. The

results are presented in Fig. 15. It can be observed from the figure that as the curing progresses, the equivalent spring stiffness increases, reaching an asymptotic value of about 115% higher than the first recorded value (four days after casting). After 28 days, the increase in the equivalent spring stiffness was about 80%. Experimental results of Malhotra (1976) show an increase of only about 7% in the ultrasonic pulse velocity between day 4 and day 10. On the other hand, in our experiment, a much higher increase of 60% was observed between day 4 and day 10. This establishes the superior performance of the present method than the ultrasonic pulse velocity technique for monitoring curing of concrete.

This new method, which requires only one surface of concrete, can be easily applied in the construction industry to decide the time of removal of the form work. It can also be utilized to determine the time of commencement of prestressing operations in the prestressed concrete members. In addition, numerous other industrial processes, which involve such curing (of materials other than concrete, such as adhesives), can also benefit from this method.

6. IMPEDANCE-BASED DAMAGE MODEL FOR CONCRETE

6.1 Definition of Damage Variable

It has been shown that in the frequency range 60-100 kHz, concrete essentially behaves as a parallel spring-damper combination. The equivalent stiffness '*k*' has been found to be a damage sensitive parameter. This section deals with calibrating '*k*' against damage using the data obtained from compression tests on concrete cubes of strengths ranging from moderate to high values.

In general, any damage to concrete causes reduction in the equivalent spring stiffness as identified by a piezo-impedance transducer. At j^{th} frequency, the associated damage variable, D_j, can be defined as

$$D_j = 1 - \frac{k_{dj}}{k_{oj}} \tag{19}$$

where k_{oj} is the equivalent spring stiffness at the j^{th} measurement point in the pristine state and k_{dj} represents the corresponding value after damage. It should be noted that $0 < D_j < 1$. Thus, D_j measures the extent of 'softening' of the identified equivalent stiffness due to damage and is expected to increase in magnitude with damage severity. The host structure can be deemed to fail if D exceeds a critical value D_c. However, from the tests on concrete cubes, it was found that it is not possible to define a unique value of D_c due to unavoidable uncertainties related to concrete, its constituents and the PZT patches. Therefore, it is proposed to define the critical value of the damage variable using the theory of fuzzy sets.

A fuzzy set is defined as a class of objects with continuum grades of membership. Such a set is characterized by a *membership (or characteristic) function*, which assigns to each object, a grade of membership ranging from 0 to 1. The membership functions represent the subjective degree of preference of a decision maker within a given tolerance. The determination of a fuzzy membership function is the most difficult as well as the most controversial part of applying the theory of fuzzy sets for solving engineering problems. Most common shapes are linear, half concave, exponential, triangular, trapezoidal, parabolic, sinusoidal and the extended π-shape (Valliappan and Pham 1993; Wu *et al.* 1999). The choice of the particular shape depends on the opinion of the expert, since there is no hard and fast rule to ascertain which shape is more realistic than the others.

In general, if *p(D)* is the probability density function for describing a structural failure event *D*, the failure probability may be expressed as

$$P_f = \int_S p(D)dD \tag{20}$$

where '*S*' is the space of the structural failure event. On the other hand, if the failure space is a fuzzy set with a membership function $f_m(D)$, the fuzzy failure probability could then be expressed as (Wu *et al.* 1999)

$$P_f = \int_S f_m(D)\, p(D)dD \tag{21}$$

This principle is used presently in evaluating concrete damage presently.

6.2 Statistical Analysis of Damage Variable for Concrete

Coming back to damage diagnosis in concrete, Fig. 16 shows the equivalent spring stiffness calculated various load ratios for five cubes labelled as C17, C43, C52, C60 and C86. Damage variables were computed at each frequency in the interval 60-100 kHz, corresponding to each load ratio, for all the five cubes. Statistical examination of the data pertaining to the damage variable indicated that it followed a normal probability distribution, for which the probability density function is given by (Kreyszig 1996)

$$p(x) = \frac{1}{\sigma\sqrt{2\pi}} e^{-\frac{(x-\mu)^2}{2\sigma^2}} \tag{22}$$

This is verified by Fig. 17, which shows the empirical cumulative probability distribution of *D* and also the theoretical normal probability distribution for all the cubes at or near failure. It is found that the distribution of the damage variable fits very well into the normal distribution. The adequacy of the normal distribution was quantitatively tested by

Kolmogorov-Smirnov goodness-of-fit test technique (Wu *et al.* 1999) and the normal distribution was found to be acceptable under a 85% confidence level for all the cubes.

6.3 Fuzzy Probabilistic Damage Calibration of Piezo-Impedance Transducers

According to the theory of continuum damage mechanics, an element is deemed to fail if $D > D_c$. As pointed out earlier, instead of defining a unique value of the critical damage variable D_c (which is a random variable), we are employing a fuzzy definition to take uncertainties into account. Using the fuzzy set theory, a fuzzy region may be defined in the interval (D_L, D_U) where D_L and D_U respectively represent the lower and the upper limits respectively of the fuzzy region (Valliappan and Pham 1993; Wu *et al.* 1999). $D > D_U$ represents a failure region with 100% failure possibility and $D < D_L$ represents a safe region with 0% failure possibility. Within the fuzzy or the transition region, that is $D_L < D < D_U$, the failure possibility could vary between 0% and 100%. A characteristic or a membership function f_m could be defined ($0< f_m(D)<1$) to express the grade of failure possibility within the region (D_L, D_U). The fuzzy failure probability can then be determined, from Eq. (21), as

$$P_f = P(D \geq D_C) = \int_{D=0}^{D=1} f_m(D)\, p(D) dD \tag{23}$$

where *p(D)* is the probability density function of the damage variable *D*, which in the present case complies with normal distribution. Based on the observations during concrete cube compression tests, D_L and D_U were chosen as 0.0 and 0.40 respectively. Further, sinusoidal function, given by the following equation, and illustrated in Fig. 18, was adopted as the membership function

$$f_m = 0.5 + 0.5\sin\left[\frac{\pi}{(D_U - D_L)}(D - 0.5D_U - 0.5D_L)\right] \tag{24}$$

This function reflects the observed trend in transducer response (in terms of damage variable based on ‘identified’ equivalent stiffness). From practical experience, it has been observed that the damage variable typically follows the trend similar to an S-curve, i.e. rising steeply with damage progression after an initial flatness and then attaining saturation. This is well represented well by the sinusoidal membership function.

Making use of this membership function, the fuzzy failure probability (FFP) was worked out for the five concrete cubes at each load ratio. A load ratio of 40% can be regarded as incipient damage since the concrete is expected to be under ‘working load’. The concrete cubes were found to exhibit a fuzzy failure probability of less than 30% at this load ratio. On the other hand, after a load ratio of 80%, the concrete cubes can be expected to be under ‘ultimate loads’. At this stage, all the cubes exhibited a fuzzy failure probability of greater than 80%, irrespective of the wide range of ultimate stresses. This is illustrated in Fig. 19. Fig. 20 shows the FFP of the cubes at intermediate stages during the tests. Based on the observations during the tests on concrete cubes, following classification of damage is recommended for various ranges of FFP.

(1) FFP < 30%	Incipient Damage (Micro-cracks)
(2) 30% < FFP < 60%	Moderate damage (Cracks start opening up)
(3) 60% < FFP < 80%	Severe damage (large visible cracks)
(4) FFP > 80%	Imminent failure

Thus, the fuzzy probabilistic approach quantifies the extent of damage on a uniform 0-100% scale. This can be employed to evaluate damage in real-life concrete structures.

7. DISCUSSION

All the PZT patches exhibited more or less a uniform behaviour with damage progression in concrete, although the strength of concrete cubes varied from as low as 17 MPa to as high as 86 MPa. Thus, the patches were subjected to a wide range of mechanical stresses and strains during the tests. At a load ratio of 1.0, almost same order of FFP is observed, irrespective of the absolute load or stress level .

In general, the PZT material shows very high compressive strength, typically over 500 MPa and it essentially exhibits a linear stress-strain relation up to strains as high as 0.006 (Cheng and Reece 2001). In our experiments conducted on concrete cubes, the strain level never exceeded 0.003 (50% of the linear limit). Also, it was observed that in all the cubes tested, the damage typically initiated near the edges of the cube and propagated to regions near the PZT patch with increasing load ratios. After failure of the cubes, all the PZT patches were found intact. Fig. 21 shows close ups of the cubes after the tests. Thus, it is evident that the sensor response reflected more the damage to the surrounding concrete rather than damage to the sensor itself. In general, we can expect such good performance in materials like concrete which are characterized by low strength as compared to the PZT patches. Hence, damage to concrete is likely to occur first, rather than to the PZT patch.

8. CONCLUSIONS

This paper presented a new impedance based NDE method for concrete, covering both strength prediction and damage assessment. A new experimental technique has been developed to determine *in situ* concrete strength non-destructively using the EMI principle. The new technique is much superior to the existing strength prediction techniques such as the

ultrasonic pulse velocity methods. The new method demands only one free surface of the specimen against two opposite surfaces in the ultrasonic methods.

It has been found that in the frequency range 60-100 kHz, concrete essentially behaves as a parallel spring damper combination. The equivalent spring stiffness tends to reduce and the damping tends to increase with damage progression. The equivalent stiffness undergoes a uniform and consistent trend, and is very suitable for diagnosing damages ranging from incipient to very severe types. A fuzzy probability based damage model has been proposed based on the equivalent stiffness extracted from the tests conducted on concrete cubes. This has enabled the calibration of the piezo-impedance transducers in terms of damage severity and can serve as a practical empirical phenomenological damage model for concrete.

In addition, this paper demonstrated the feasibility of monitoring curing of concrete using the EMI technique, with a much higher sensitivity than the conventional methods. This technique can be easily applied in the construction industry to decide the appropriate time of removal of the formwork and the time of commencement of prestressing in the concrete members.

ACKNOWLEDGEMENTS

The authors gratefully acknowledge the kind help and assistance provided by Mr. Say Ian Lim and Mr. Kian Tiong Goo in performing many of the experiments reported in this paper as a part of their final year projects. Thanks are also due to Associate Professor Swee-Chuan Tjin and Mrs. Rupali Suresh for providing optical fibre pieces for controlling epoxy thickness.

REFERENCES

Aktan, A. E., Catbas, F. N., Grimmelsman, K. A. and Tsikos, C. J. (2000), "Issues in Infrastructure Health Monitoring for Management", Journal of Engineering Mechanics, ASCE, Vol. 126, pp. 711-724.

Ayres, J. W., Lalande, F., Chaudhry, Z., and Rogers, C. A. (1998), "Qualitative Impedance-Based Health Monitoring of Civil Infrastructures," Smart Materials and Structures, Vol. 7, pp. 599-605.

Bhalla, S. and Soh, C. K. (2003), "Structural Impedance Based Damage Diagnosis by Piezo-Transducers," Earthquake Engineering and Structural Dynamics, Vol. 32, pp. 1897-1916.

Bhalla, S. and Soh, C.K. (2004a), "High Frequency Piezoelectric Signatures for Diagnosis of Seismic/ Blast Induced Structural Damages," NDT&E International, Vol. 37, pp. 23-33.

Bhalla, S. and Soh, C.K. (2004b), "Structural Health monitoring by Piezo-Impedance Transducers: I Modeling," Journal of Aerospace Engineering, ASCE, Vol. 17, No. 4, pp. 154-165.

Bhalla, S. and Soh, C.K. (2004c), "Structural Health monitoring by Piezo-Impedance Transducers: II Applications," Journal of Aerospace Engineering, ASCE, ASCE, Vol. 17, No. 4, pp. 166-175.

Bungey, J. H. (1982), The Testing of Concrete in Structures, Surrey University Press.

Cheng, B. L. and Reece, M. J. (2001), "Stress Relaxation and Estimation of Activation Volume in a Commercial Hard PZT Piezoelectric Ceramic", Bulletin of Material Science, Indian Academy of Sciences, Vol. 24, No. 2, pp. 165–167.

Farrar, C. R. and Jauregui, D. A. (1998), "Comparative Study of Damage Identification Algorithms Applied to a Bridge: I. Experiment", Smart Materials and Structures, Vol. 7, pp. 704-719.

Giurgiutiu, V. and Rogers, C. A., (1997), "Electromechanical (E/M) Impedance Method for Structural Health Monitoring and Non-Destructive Evaluation", Proceedings of International Workshop on Structural Health Monitoring, edited by F. K. Chang, Stanford University, Stanford, California, September 18-20, Technomic Publishing Co., pp. 433-444.

Giurgiutiu, V. and Zagrai, A. N. (2000), "Characterization of Piezoelectric Wafer Active Sensors", Journal of Intelligent Material Systems and Structures, Vol. 11, pp. 959-976.

Giurgiutiu, V. and Zagrai, A. N. (2002), "Embedded Self-Sensing Piezoelectric Active Sensors for On-Line Structural Identification", Journal of Vibration and Acoustics, ASME, Vol. 124, pp. 116-125.

Kawiecki, G. (2001), "Modal damping Measurement for Damage Detection", Smart Materials and Structures, Vol. 10, pp. 466-471.

.

Kreyszig, E. (1993), Advanced Engineering Mathematics, 7th Ed., Wiley, New York.

Liang, C., Sun, F. P. and Rogers, C. A. (1994) "Coupled Electro-Mechanical Analysis of Adaptive Material Systems- Determination of the Actuator Power Consumption and System Energy Transfer," Journal of Intelligent Material Systems and Structures, Vol. 5, pp. 12-20.

Malhotra, V. M. (1976), Testing Hardened Concrete: Nondestructive Methods, American Concrete Institute (ACI) Monograph No. 9.

Pandey, A. K., Biswas, M. and Samman, M. M. (1991), "Damage Detection from Changes in Curvature Mode Shapes", Journal of Sound and Vibration, Vol. 145, pp. 321-332.

Pandey, A. K. and Biswas, M. (1994), "Damage Detection in Structures Using Changes in Flexibility", Journal of Sound and Vibration, Vol. 169, No. 1, pp. 3-17.

Park, G., Cudney, H. H. and Inman, D. J. (2000), "Impedance-Based Health Monitoring of Civil Structural Components," Journal of Infrastructure Systems, ASCE, Vol. 6, pp. 153-160.

Park, G., Cudney, H. H., and Inman, D. J. (2001) “Feasibility of Using Impedance-Based Damage Assessment for Pipeline Structures,” Earthquake Engineering and Structural Dynamics, Vol. 30, pp. 1463-1474.

Park, G., Sohn, H., Farrar, C. R. and Inman, D. J. (2003), “Overview of Piezoelectric Impedance-Based Health Monitoring and Path Forward”, The Shock and Vibration Digest, Vol. 35, pp. 451-463.

PI Ceramic (2004), Lindenstrabe, Germany, http://www.piceramic.de.

RS Components (2004), Northants, UK, http://www.rs-components.com.

Soh, C. K., Tseng, K. K. H., Bhalla, S. and Gupta, A. (2000) “Performance of Smart Piezoceramic Patches in Health Monitoring of a RC Bridge,” Smart Materials and Structures, Vol. 9, pp. 533-542.

Sun, F. P., Chaudhry, Z., Rogers, C. A., Majmundar, M. and Liang, C. (1995) “AutomatedReal-Time Structure Health Monitoring via Signature Pattern Recognition,” Proceedings of SPIE Conference on Smart Structures and Materials, edited by I. Chopra, San Diego, California, Feb.27-Mar1, SPIE Vol. 2443, pp. 236-247.

Valliappan, S. and Pham, T. D. (1993), “Fuzzy Finite Element Analysis of a Foundation on an Elastic Soil Medium”, International Journal for Numerical and Analytical Methods on Geomechanics, Vol. 17, pp. 771-789.

Wu, C. Q., Hao, H. and Zhou, Y. X. (1999), “Fuzzy-Random Probabilistic Analysis of Rock Mass Responses to Explosive Loads”, Computers and Geotechnics, Vol. 25, pp. 205-225.

Zimmerman, D. C. and Kaouk, M. (1994), “Structural Damage Detection Using a Minimum Rank Update Theory”, Journal of Vibration and Acoustics, Vol. 116, pp. 222-231

LIST OF FIGURES AND TABLES

Fig. 1 Modelling PZT-structure electro-mechanical impedance interaction.

Fig. 2 Admittance spectra for free and fully clamped PZT patches.

(a) Conductance (G) vs frequency. (b) Susceptance (B) vs frequency.

Fig. 3 (a) Optical fibre pieces laid on concrete surface before applying adhesive.

(b) Bonded PZT patch.

Fig. 4 Effect of concrete strength on first resonant frequency of PZT patch.

(a) Conductance vs frequency. (b) Susceptance vs frequency.

Fig. 5 Correlation between concrete strength and first resonant frequency.

Fig. 6 Equivalent system 'identified' by PZT patch.

Fig. 7 Impedance plots for concrete cube C43.

(a) Real component of mechanical impedance (x) vs frequency.

(b) Imaginary component of mechanical impedance (y) vs frequency.

Fig. 8 Experimental set-up for inducing damage on concrete cubes.

Fig. 9 Conductance signatures of PZT patch bonded to cube C43 at various load levels (LR stands for 'load ratio').

Fig. 10 Load histories of four concrete cubes.

(a) C17 (b) C43 (c) C52 (d) C86

Fig. 11 Correlation between loss of secant modulus and loss of equivalent spring stiffness with damage progression.

(a) C17 (b) C43 (c) C52 (d) C86

Fig. 12 Changes in equivalent damping and equivalent stiffness for cube C43.

Fig. 13 Short-term effect of concrete curing on conductance signatures.

Fig. 14 Long-term effect of concrete curing on conductance signatures.

Fig. 15 Effect of concrete curing on equivalent spring stiffness.

Fig. 16 Effect of damage on equivalent spring stiffness (LR stands for 'Load ratio').

(a) C17 (b) C43 (c) C52 (d) C60 (e) C86

Fig. 17 Theoretical and empirical probability density functions near failure.

(a) C17 (b) C43 (c) C52 (d) C60 (e) C86

Fig. 18 Sinusoidal membership function.

Fig. 19 Fuzzy failure probabilities of concrete cubes at incipient damage level and at failure stage.

Fig. 20 Fuzzy failure probabilities of concrete cubes at various load levels.

Fig. 21 Cubes after the test. (a) C17 (b) C43 (c) C52 (d) C60 (e) C86

Table 1 Averaged parameters of test sample of PZT patches.

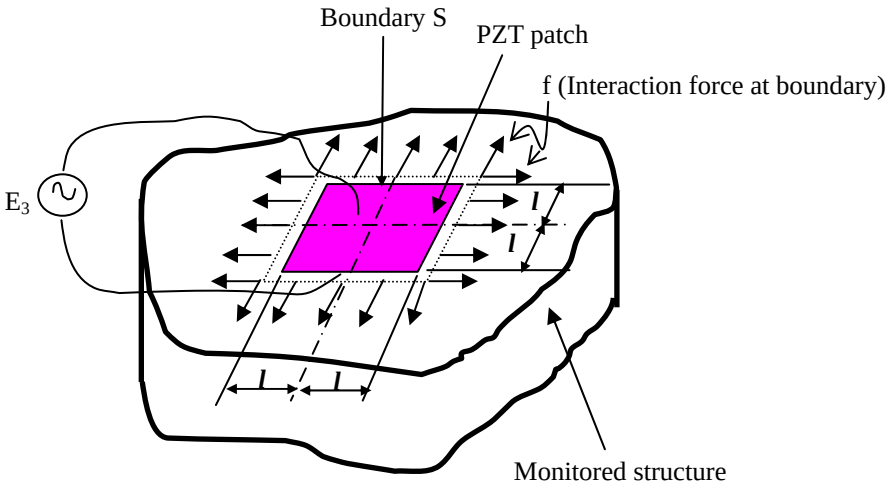

Fig. 1 Modelling PZT-structure electro-mechanical impedance interaction.

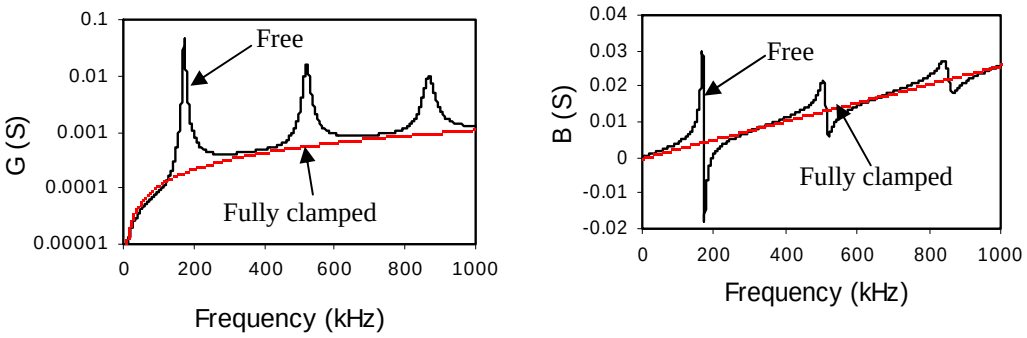

Fig. 2 Admittance spectra for free and fully clamped PZT patches.
(a) Conductance (G) vs frequency. (b) Susceptance (B) vs frequency.

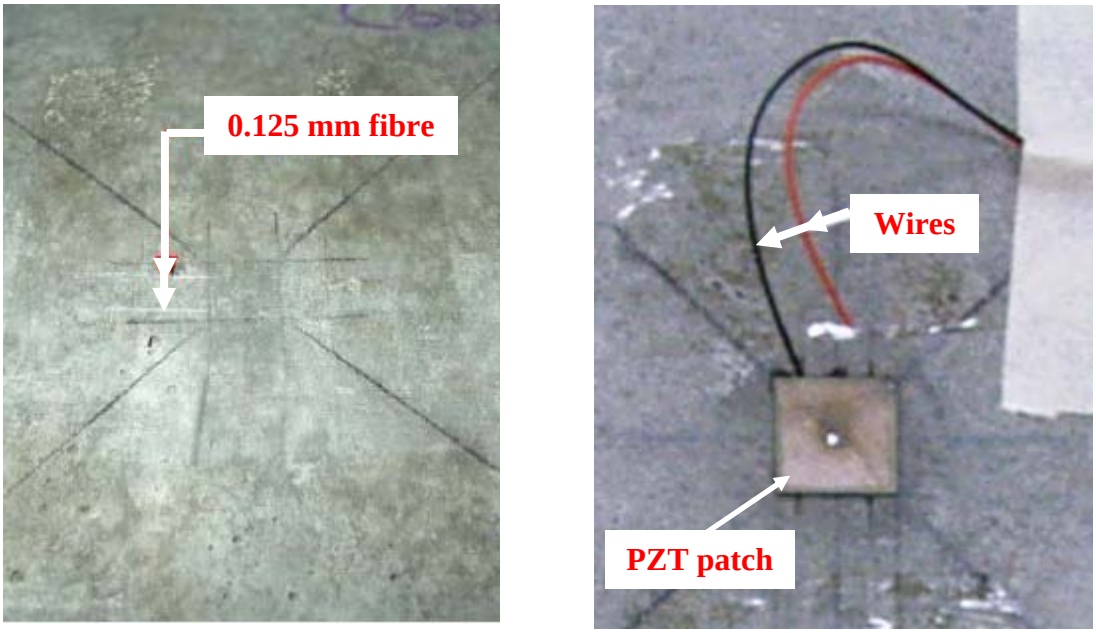

Fig. 3 (a) Optical fibre pieces laid on concrete surface before applying adhesive.
(b) Bonded PZT patch.

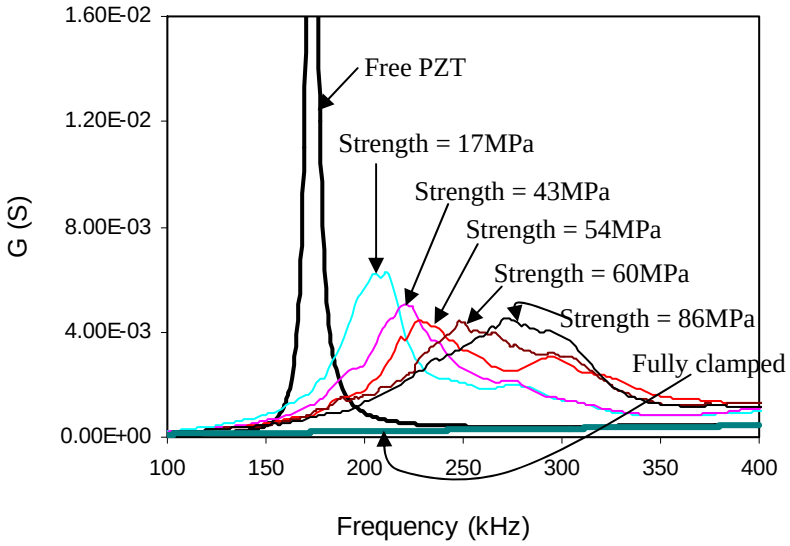

(a)

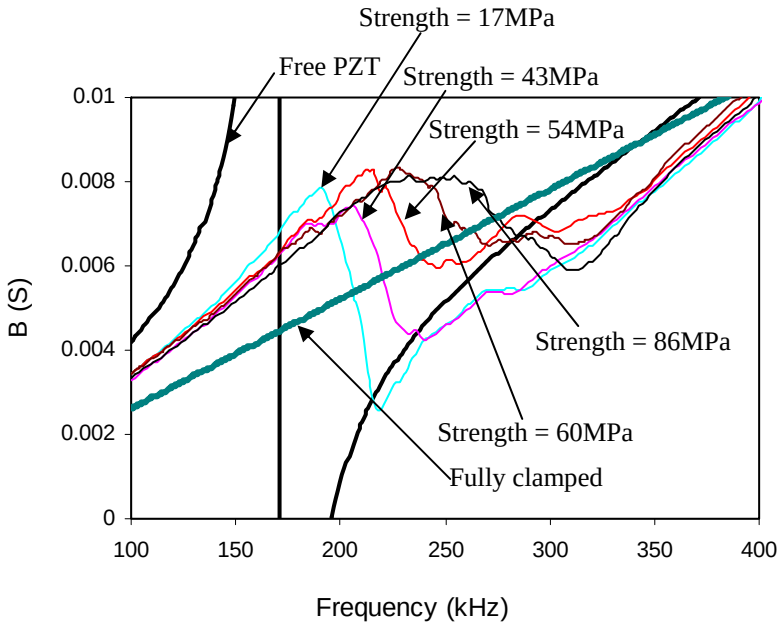

(b)

Fig. 4 Effect of concrete strength on first resonant frequency of PZT patch. (a) Conductance vs frequency. (b) Susceptance vs frequency.

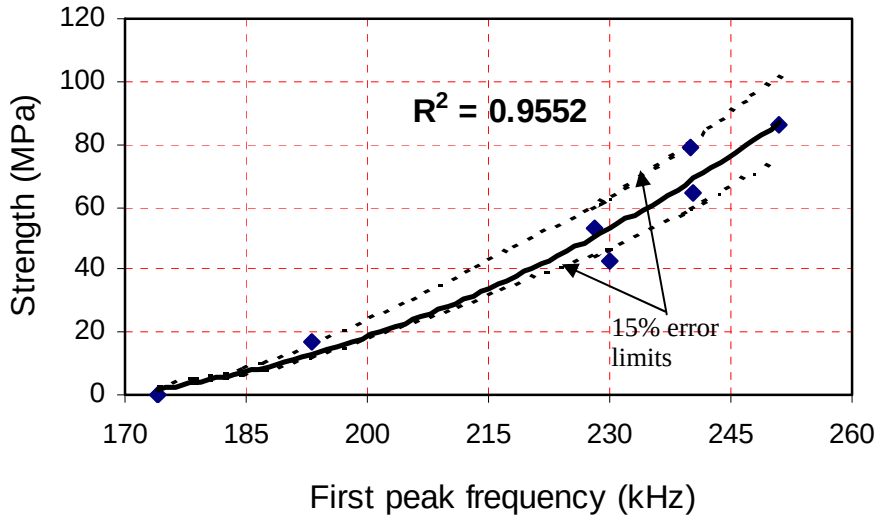

Fig. 5 Correlation between concrete strength and first resonant frequency.

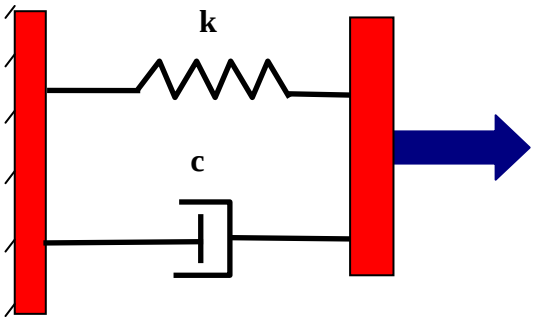

Fig. 6 Equivalent system ‘identified’ by PZT patch.

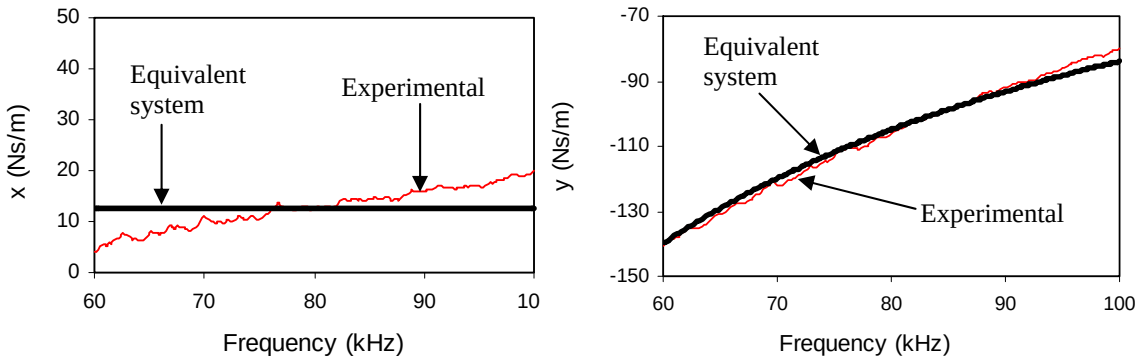

(a) (b)

Fig. 7 Impedance plots for concrete cube C43.

(a) Real component of mechanical impedance (x) vs frequency.

(b) Imaginary component of mechanical impedance (y) vs frequency.

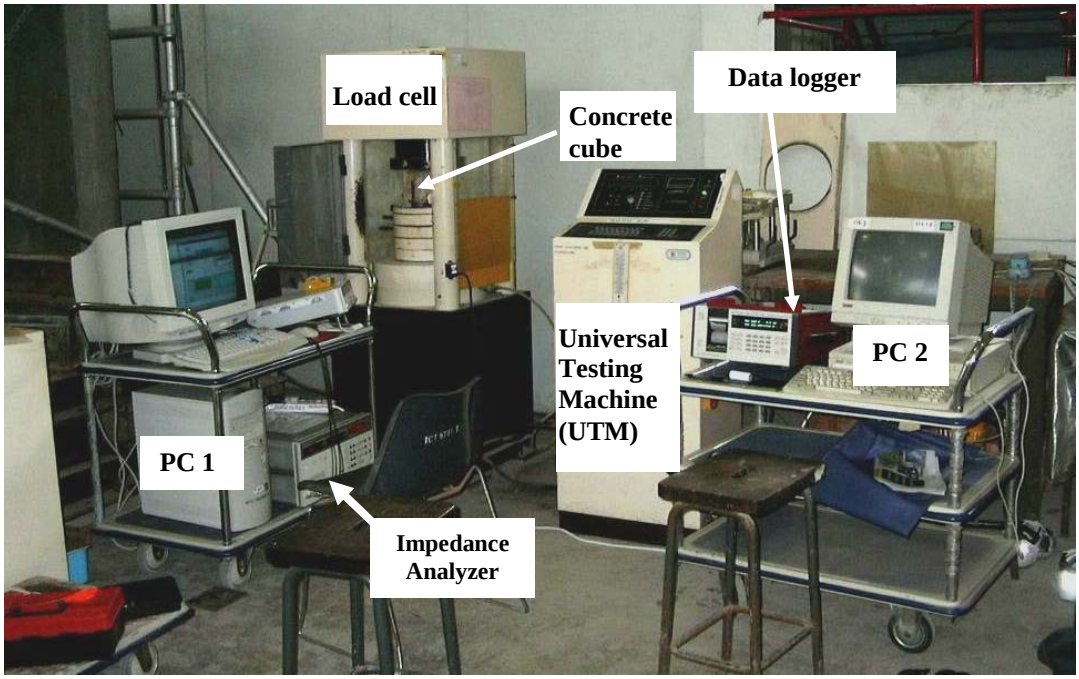

Fig. 8 Experimental set-up for inducing damage on concrete cubes.

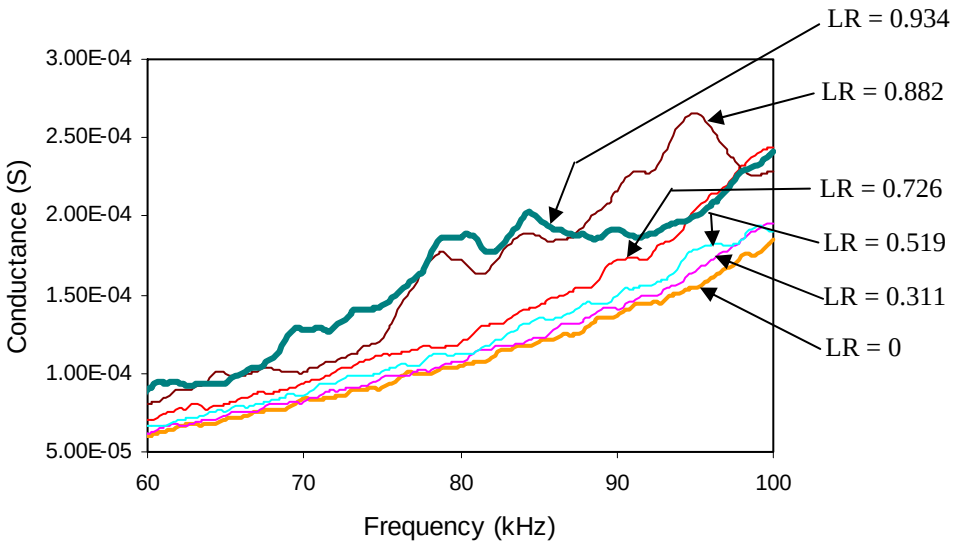

Fig. 9 Conductance signatures of PZT patch bonded to cube C43 at various load levels (LR stands for 'load ratio').

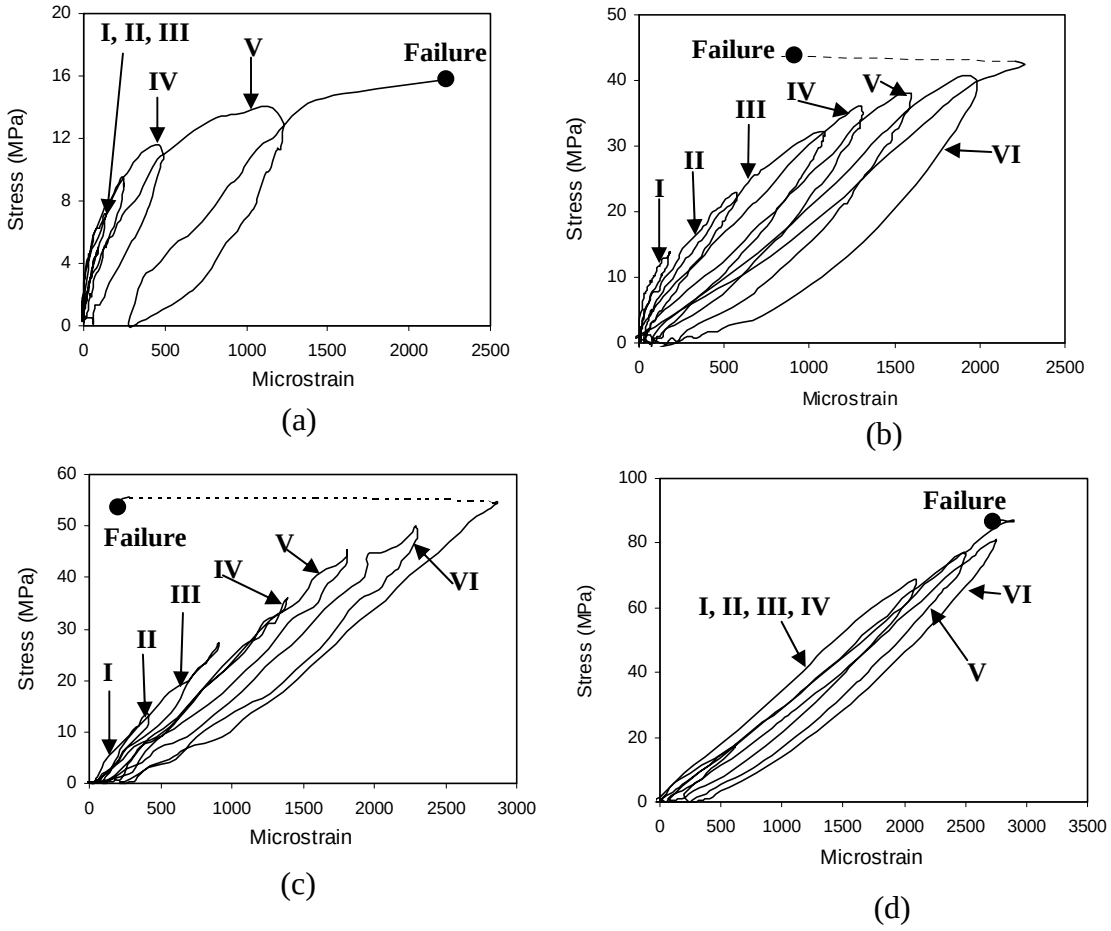

Fig. 10 Load histories of four concrete cubes.

(a) C17 (b) C43 (c) C52 (d) C86

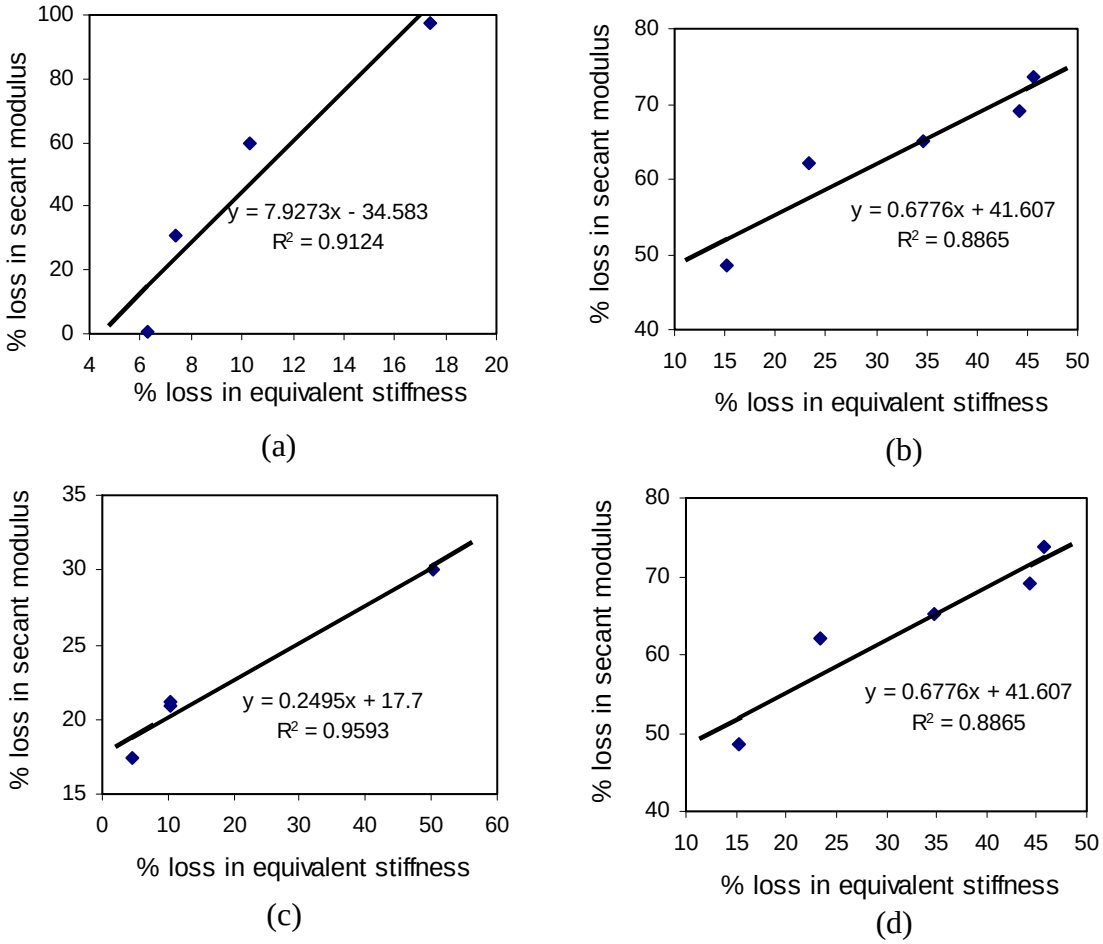

Fig. 11 Correlation between loss of secant modulus and loss of equivalent spring stiffness with damage progression.
(a) C17 (b) C43 (c) C52 (d) C86

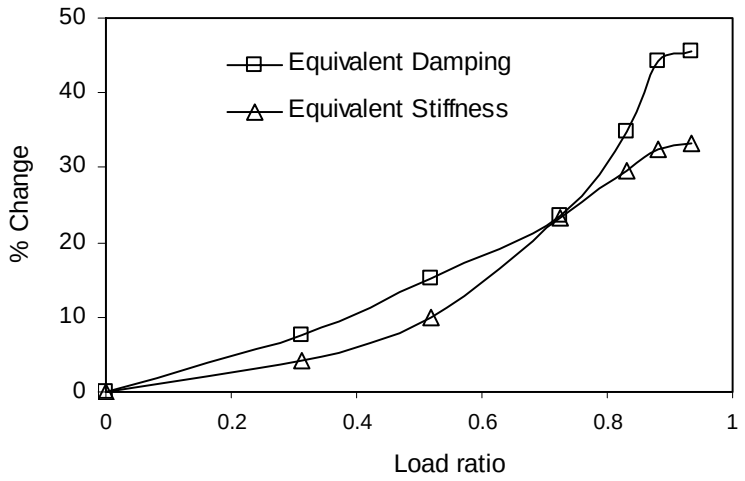

Fig. 12 Changes in equivalent damping and equivalent stiffness for cube C43.

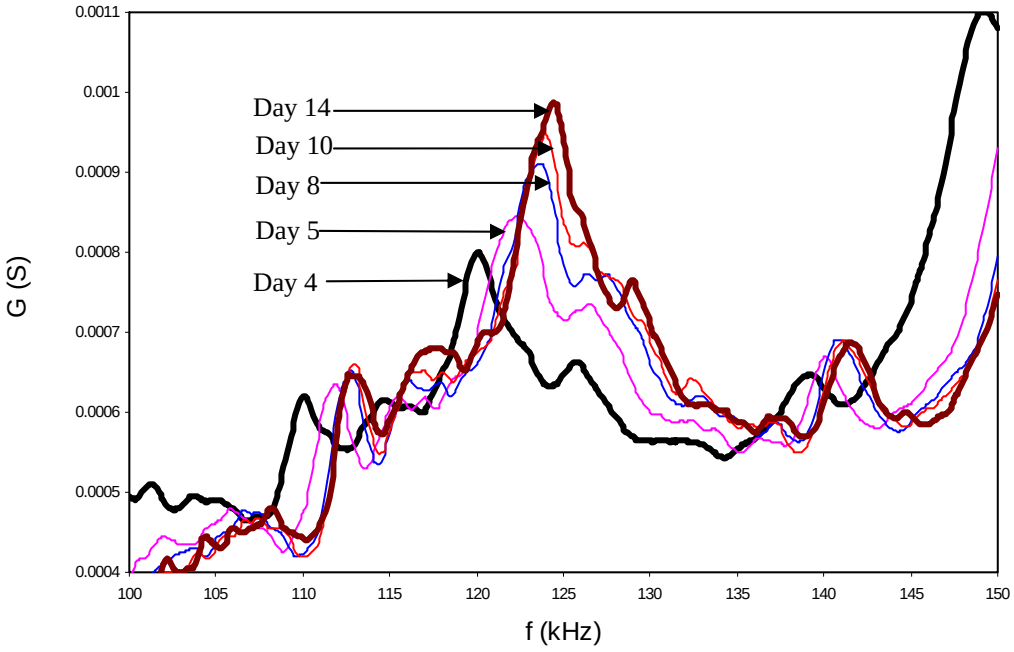

Fig. 13 Short-term effect of concrete curing on conductance signatures.

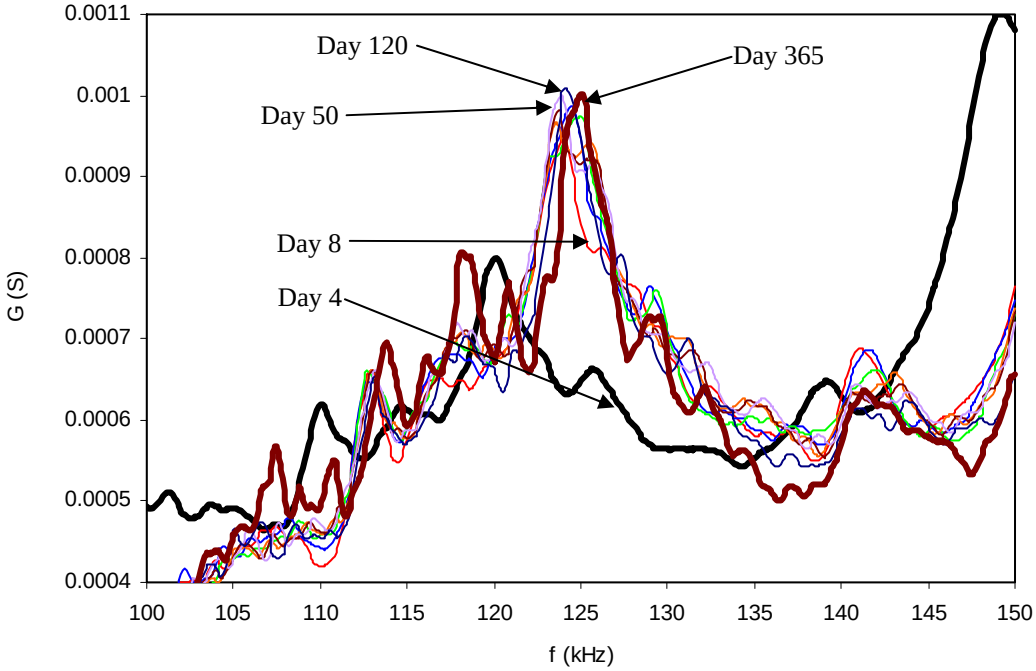

Fig. 14 Long-term effect of concrete curing on conductance signatures.

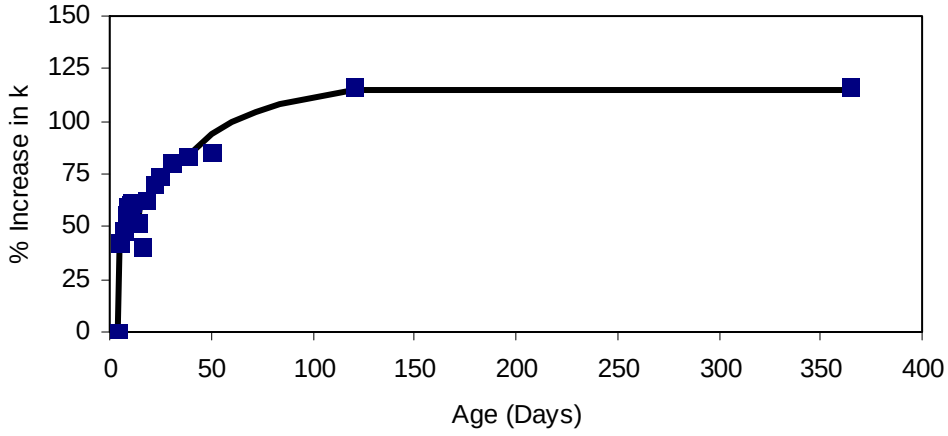

Fig. 15 Effect of concrete curing on equivalent spring stiffness.

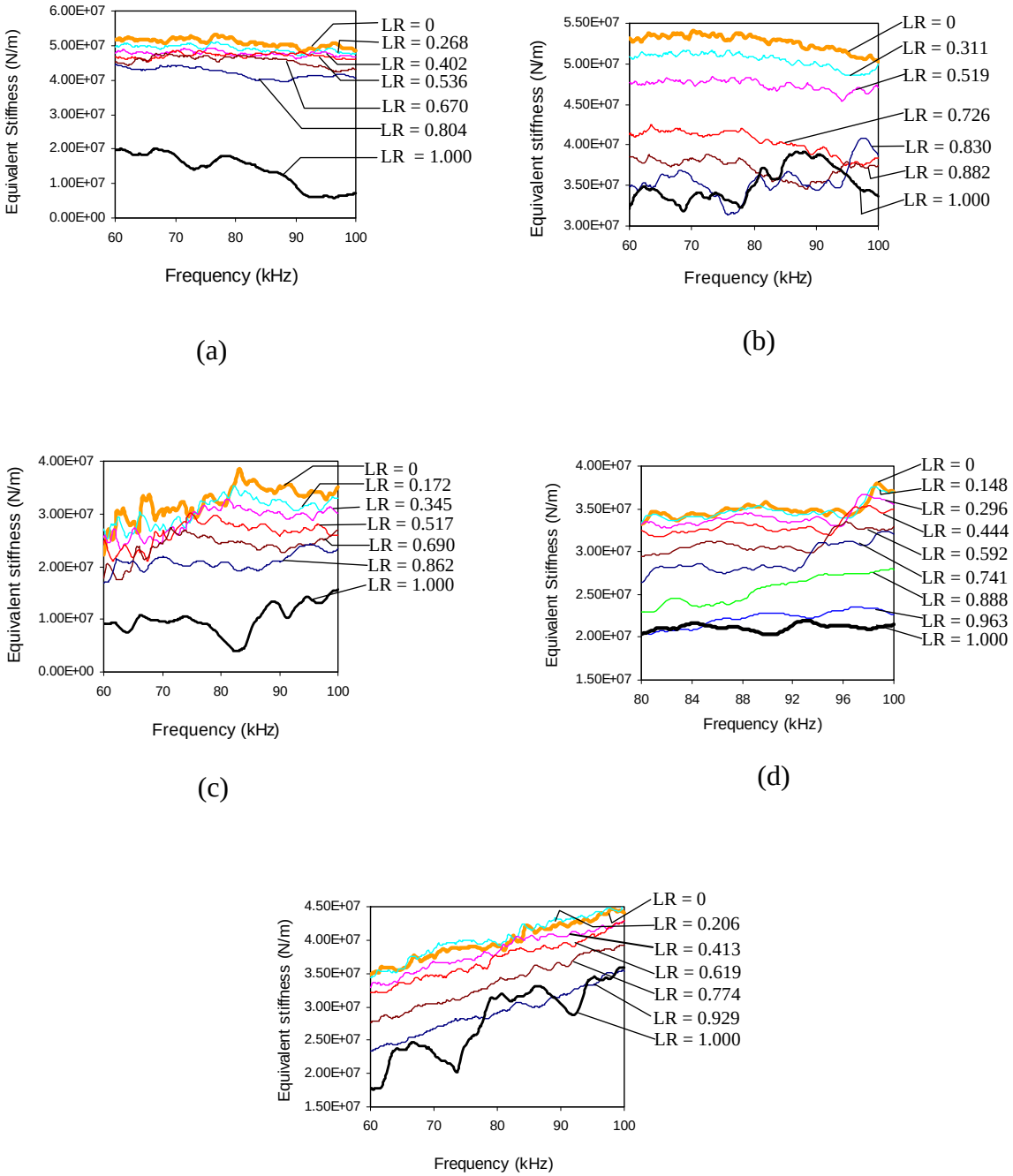

Fig. 16 Effect of damage on equivalent spring stiffness (LR stands for 'Load ratio').
(a) C17 (b) C43 (c) C52 (d) C60 (e) C86

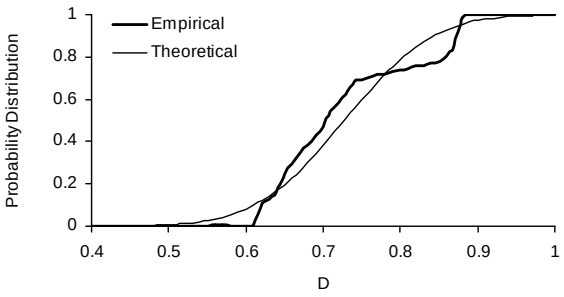

(a)

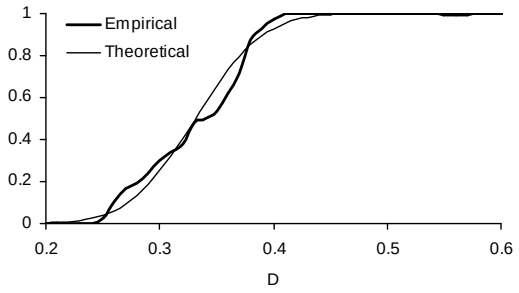

(b)

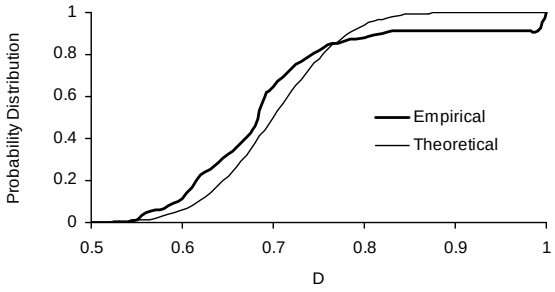

(c)

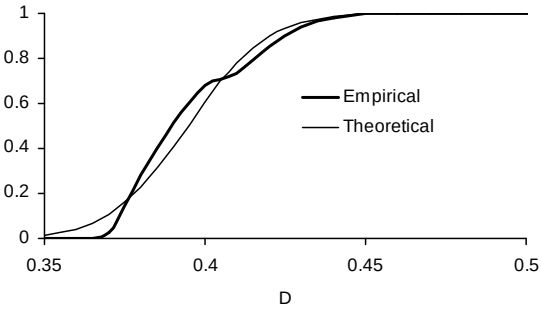

(d)

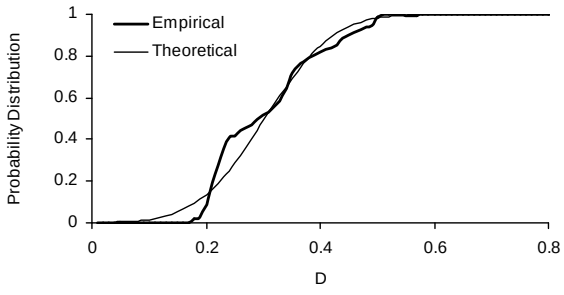

(e)

Fig. 17 Theoretical and empirical probability density functions near failure.
(a) C17 (b) C43 (c) C52 (d) C60 (e) C86

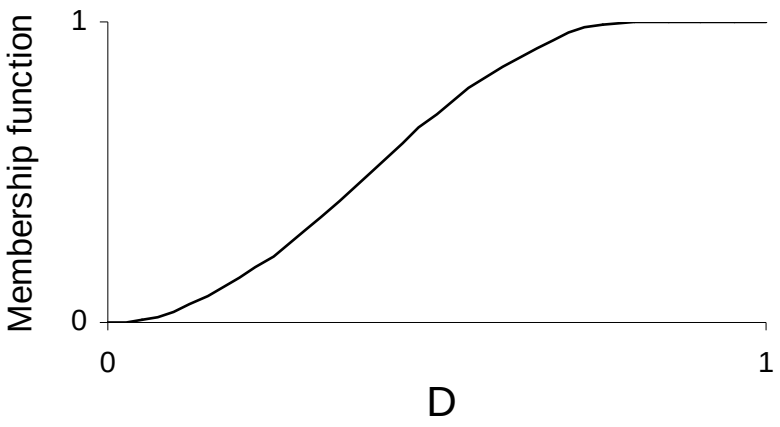

Fig. 18 Sinusoidal membership function.

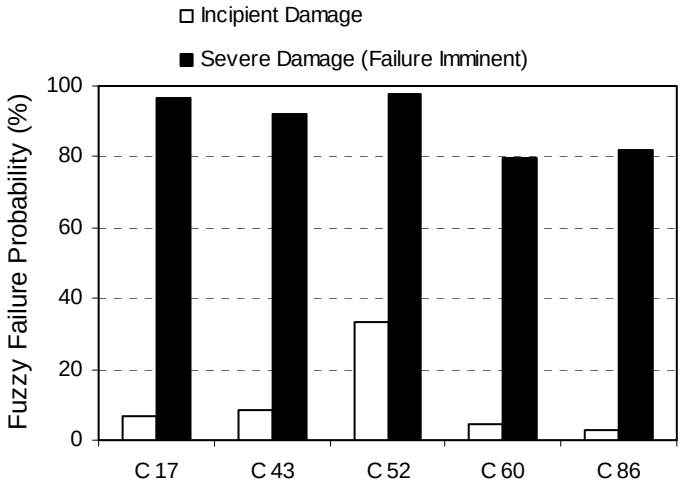

Fig. 19 Fuzzy failure probabilities of concrete cubes at incipient damage level and at failure stage.

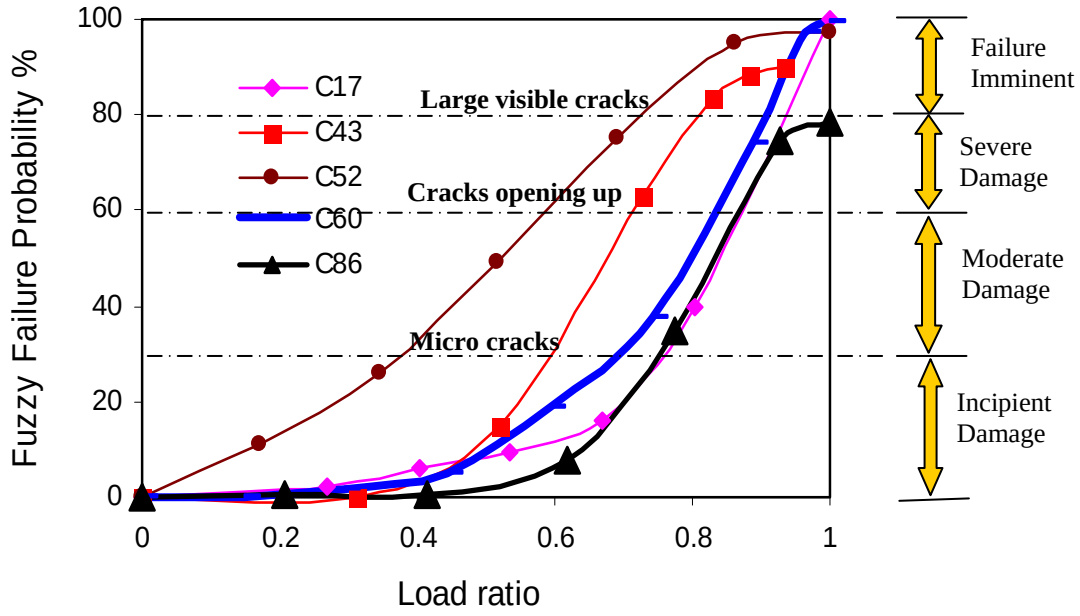

Fig. 20 Fuzzy failure probabilities of concrete cubes at various load levels.

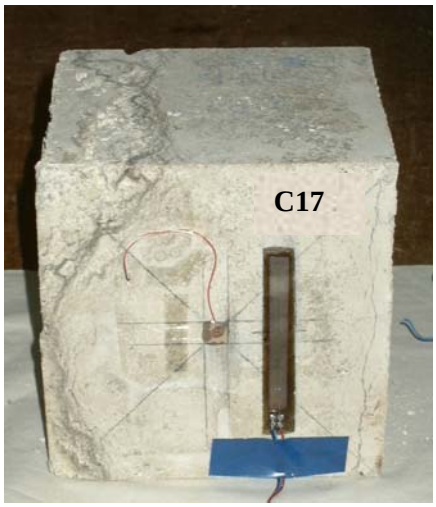

(a)

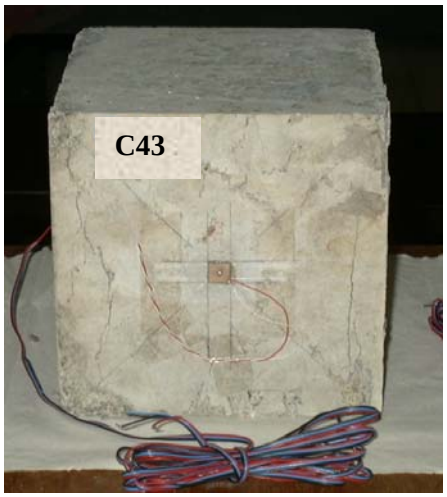

(b)

(c)

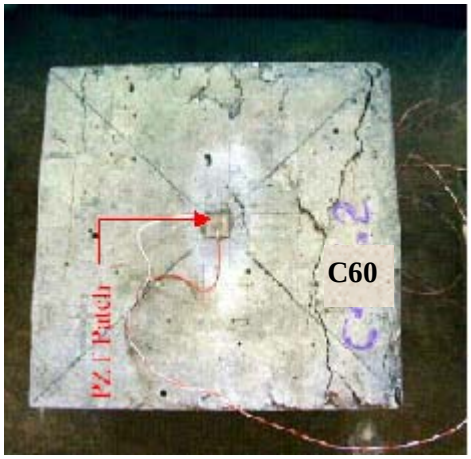

(d)

(e)

Fig. 21 Cubes after the test. (a) C17 (b) C43 (c) C52 (d) C60 (e) C86.

Table 1 Averaged parameters of test sample of PZT patches.

Physical Parameter	Value
Electric Permittivity, ε_{33}^{T} (farad/m)	1.7785×10^{-8}
Peak correction factor, C_f	0.898
$K = \frac{2d_{31}^2 Y^E}{(1-\upsilon)}$ (NV^{-2})	5.35×10^{-9}
Piezoelectric strain coefficient (mV^{-1})	-2.1×10^{10}
Mechanical loss factor, η	0.0325
Dielectric loss factor, δ	0.0224